Suppression of electron injection into a finite superlattice in an applied magnetic field

A. A. Krokhin,* T. M. Fromhold, A. E. Belyaev, H. M. Murphy, L. Eaves, D. Sherwood, P. C. Main, and M. Henini
School of Physics and Astronomy, University of Nottingham, Nottingham NG7 2RD, United Kingdom
(Received 7 September 2000; published 30 April 2001)

We present experimental and theoretical studies of the current-voltage characteristics, $I(V)$, of undoped GaAs/(Al_xGa_{1-x})As superlattices (SL's) in a strong magnetic field **B** applied parallel to the growth axis. A series of $I(V)$ characteristics measured at $B=1,2,\ldots,10$ T shows that increasing the magnetic field gradually suppresses the current across the whole range of V. We show that at low V this suppression originates from a decrease in the rate of injection of carriers into the SL from the heavily doped emitter contact. Because the chemical potential in the emitter contact lies below the lowest miniband of the SL, electrons enter the SL by tunneling through a triangular potential barrier formed by the miniband edge. The tunneling rate depends on V and on the electron energy for longitudinal motion along the SL axis. The latter is reduced (by at least $\hbar\omega_c/2$, where ω_c is the cyclotron frequency) in the magnetic field. Consequently, the tunneling rate decreases with increasing **B**. This mechanism of suppression dominates at low voltages ($V<40$ mV) when the barrier transmission coefficient is low.

DOI: 10.1103/PhysRevB.63.195323 PACS number(s): 73.21.−b, 73.61.−r

I. INTRODUCTION

Electron transport in semiconductor superlattices (SL's) has been an active research field since the pioneering work of Esaki and Tsu.[1] The interest in this area is partly due to the nonlinearity of the current-voltage characteristics $I(V)$ of a SL. Many SL's exhibit a peak in the miniband current followed by a region of negative differential conductance. Although the nature of the negative differential conductance is well understood, the details and the form of the $I(V)$ characteristics over wide voltage ranges lacks a complete explanation. The effects of temperature and external magnetic field are also not fully understood.

A strong magnetic field **B** applied parallel to the SL axis leads to Landau quantization of electron states in both the contacts and the SL layers. Then the in-plane Landau states and longitudinal Wannier-Stark states are coupled by various electron-scattering mechanisms. For the SL structure considered here, optical-phonon scattering is the most effective. At high voltages this coupling gives rise to cyclotron-Stark-phonon resonance effects in the $I(V)$ characteristics.[2–7] At lower voltages, when Wannier-Stark quantization is of no importance, magnetophonon resonance oscillations have been observed[8] and studied theoretically.[9] Apart from producing sharp resonance effects in the conductivity, the magnetic field also reduces electron mobility, and thereby gives rise to a smooth positive magnetoresistance.[10,8,11]

In the present paper we study a suppression of the miniband conductivity of a GaAs/(Al_xGa_{1-x})As superlattice, which is induced by an applied magnetic field. We propose an explanation of this suppression, which has notable differences from that considered in previous work[12–14] where the magnetic field was shown to affect the probability of inelastic electron-phonon scattering. These earlier works involved numerical simulations of electron dynamics in an infinite SL, using a Monte Carlo method, and showed good agreement with experimental results for the $I(V)$ curves at high voltages. In particular, for voltages within the region of negative differential resistance, the experimental $I(V)$ curves are well reproduced by the numerical calculations. But at low voltages, when the electron energy is insufficient to emit an LO phonon, the agreement between the experiment and the theory is not so good. In this paper, we focus on that low-voltage regime, and show that the suppression originates mainly from the effect of B on the injection of conduction electrons into the SL miniband. In contrast to previous calculations,[12–14] we consider a sample of *finite* length and show that applying the magnetic field decreases the probability of an electron tunneling from the emitter contact into the SL miniband. Since the parallel magnetic field affects neither the barrier, nor the longitudinal motion of the carriers, the suppression may be explained only by a redistribution of the occupied emitter states, induced by the magnetic field. This statistical mechanism reproduces the experimental data well, and does not involve extensive numerical calculations; all of the theoretical results can be expressed in a relatively simple analytical form.

II. DESCRIPTION OF THE SL STRUCTURE AND EXPERIMENTAL RESULTS

The sample used in our experiments was grown by molecular-beam epitaxy on an *n*-type GaAs substrate. It contains 19 SL periods, which are separated from two heavily *n*-doped GaAs contacts by 10.2 nm wide undoped GaAs spacer layers. A unit cell of the SL is formed from an $(Al_xGa_{x-1}As)$ barrier of width $b=2.08$ nm and a GaAs well of width $w=9.72$ nm. The width of this unit cell defines the SL period $d=b+w$. The barriers and quantum wells are nominally undoped. Figure 1 shows a schematic conduction-band diagram for the device under zero applied voltage. The first miniband has a nominal width of $\Delta_1=12.1$ meV, and is separated from the second miniband by a minigap $E_g=98$ meV. The Fermi energy of the doped emitter contact is $E_{em}=160$ meV. At zero bias, the bottom of the first miniband is at an energy $E_1\approx 12$ meV above the chemical potential of the emitter contact, which is the origin of our energy scale (dotted line in Fig. 1). Consequently, there is a

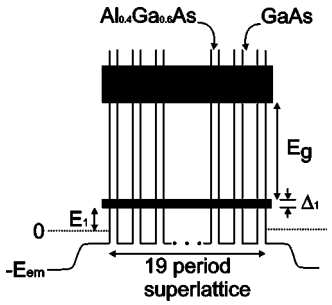

FIG. 1. Schematic conduction-band diagram of the SL for $V=0$ mV, showing the first and second minibands (shaded) and emitter/collector contacts.

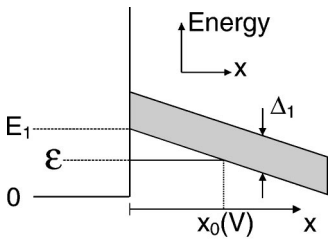

FIG. 3. Schematic diagram showing how the energy range of the first miniband (shaded) varies with position x from the left-hand edge of the SL (vertical line) under bias. Energies and positions shown are defined in the text. The origin of the energy scale is the emitter Fermi level.

potential barrier of height E_1 which, at low temperatures, prevents direct thermal excitation of an electron from the emitter contact into the first miniband. Therefore at $T=0$ K and zero voltage the device possesses no intrinsic conductance.

Since our samples are undoped, the current that flows when a finite bias voltage is applied is nonohmic. This is clearly seen from the experimental $I(V)$ characteristics shown in Fig. 2. These $I(V)$ curves were measured at $T=4.2$ K and for $B=0$ to 10 T at intervals of 1 T. The current suppression induced by the magnetic field can be seen even for a low field of $B=1$ T, and becomes more pronounced as B is increased. Note that at the low voltages, $0\leqslant V\leqslant 40$ mV shown in the main part of Fig. 2, the current increases almost exponentially with increasing V. Moreover, the suppression ratio $I(V,B)/I(V,0)$ is almost independent of voltage, as discussed in Sec. IV below.

III. ELECTRON INJECTION PROCESS–THERMAL ACTIVATION AND TUNNELING

When a bias voltage is applied, electrons move through the undoped spacer layer to the left of the SL. The electric field in this region is insufficient to quantize the electron motion normal to the layers. Consequently, the carriers in the spacer layer form a three-dimensional electron gas. Due to the difference between the Fermi level of the emitter contact and the bottom of the miniband at zero bias, carriers at the Fermi energy in the left-hand side contact have insufficient energy to enter the SL directly. They need to overcome a

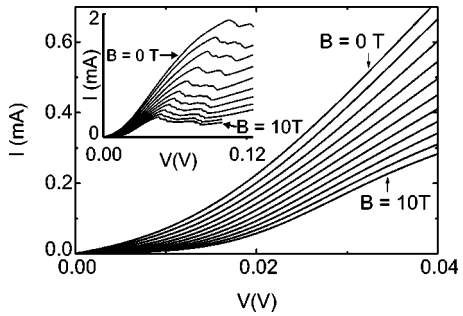

FIG. 2. $I(V)$ characteristics measured for the SL with $B=0,1,2,\ldots,10$ T. Inset shows the same $I(V)$ curves over a wider range of voltages.

potential barrier of maximum height E_1 which, according to tight-binding-model calculations, is about 12 meV for an infinite SL. The classical probability of surmounting this barrier by thermionic emission is $\exp(-E_1/kT)\approx 5\times 10^{-15}$ at $T=4.2$ K, which is too small to produce any measurable current flow through the SL. To account for the relatively large currents measured in the experiments, there must be an alternative mechanism, which is field emission. This mechanism is quantum-mechanical tunneling through the barrier produced by the edge of the lowest miniband. The tunneling rate increases rapidly with the applied voltage. This gives rise to the strongly nonlinear shapes of the $I(V)$ curves shown in Fig. 2.

The physical nature of the tunneling injection process is very similar to that of tunneling through a Schottky barrier (see reviews[15,16]) or Zener breakdown in crystal semiconductors or in SL's.[17,18] Under an applied voltage, the energy bands are tilted, which gives rise to a finite probability of tunneling between the states in the emitter contact and those in the SL miniband, as shown in Fig. 3. We measure the electron energy ε associated with motion along the SL $(x-)$ axis from the chemical potential in the emitter contact, which means that $\varepsilon > -E_{em}$ (see Fig. 1). For the finite temperature used in our experiments, electrons in the emitter contact can be thermally excited to states above the Fermi level and then tunnel from these states into the SL miniband. This type of temperature-assisted tunneling occurs in the Schottky diode in the thermionic-field emission regime.[16] The tunneling probability decreases exponentially with increasing length of the barrier x_0, which depends on ε and on the voltage V (see Fig. 3). To good approximation, the forbidden region below the first miniband forms an almost triangular barrier with transmission coefficient

$$D(\varepsilon)=\exp\left\{-\frac{4\sqrt{2m}}{3eF\hbar}(E_1-\varepsilon)^{3/2}\right\}. \tag{1}$$

Here, F is the electric field at the left-hand edge of the SL, and $m\approx 0.08m_e$ is the approximate effective mass of an electron in GaAs with an energy corresponding to the bottom of the miniband. We note that the miniband edge does not produce a simple electrostatic potential barrier for the conduction electrons. However, to enter the SL, the electron must cross the region of forbidden energies below the band edge. It was shown recently, that in the semiclassical approxima-

tion, the probability of transition through this forbidden region is equal to the probability of tunneling through the equivalent (triangular) potential barrier.[19]

The total injection current per unit area in the $y-z$ plane produced by the occupied emitter states can be written in a form similar to the current through a Schottky barrier[15] and is given by

$$j(F)=e\int_{-E_{em}}^{E_1} v_x D(\varepsilon) f(\varepsilon)\rho(\varepsilon)d\varepsilon, \tag{2}$$

where

$$f(\varepsilon)=2\int_{-\infty}^{\infty}\frac{dp_y dp_z}{h^2}\left\{1+\exp\left(\frac{\varepsilon}{kT}+\frac{p_y^2+p_z^2}{2mkT}\right)\right\}^{-1}, \tag{3}$$

is the supply function[20] of electrons in the emitter (the distribution function of electrons per unit area with energy ε associated with motion along the x axis), v_x is the electron velocity along the electric field (parallel to the x axis), $\rho(\varepsilon)$ is the density of states per unit length associated with motion along the x axis in the n^+ emitter, and p_y, p_z are momentum components for in-plane motion. The current given by Eq. (2) is derived from a coherent model of tunneling in which p_y and p_z are conserved in the tunneling process. The lower limit of the integral in Eq. (2) is determined by the energy of the conduction band edge in the emitter contact, while the upper limit is determined by the top of the triangular barrier. A small number of electrons are thermally excited to higher ε values and enter the miniband directly. But, as emphasized above, there are so few of these electrons that they make a negligible contribution to the current. For each value of ε between the upper and lower limits of integration in Eq. (2), the electron can, in principle, populate any lateral momentum state (p_y,p_z) with an occupancy determined by the Fermi-Dirac distribution in Eq. (3). Because of this, the limits of integration in Eq. (3) are unbounded.

The integral in Eq. (2) contains a product of two exponential functions: the barrier transmission coefficient $D(\varepsilon)$ and the distribution function $f(\varepsilon)$. The principal contribution to the integral comes from a narrow range of energies[21] close to the optimal tunneling energy $\varepsilon_0(F)$ that maximizes the product $D(\varepsilon)f(\varepsilon)$. From the condition $d[D(\varepsilon)f(\varepsilon)]/d\varepsilon$ we obtain a transcendental equation for the optimal energy,

$$\frac{F_c}{F}\sqrt{1-\frac{\varepsilon_0}{E_1}}=\frac{1}{1+\exp(-\varepsilon_0/kT)}, \tag{4}$$

where

$$F_c=\frac{2kT\sqrt{2mE_1}}{e\hbar}, \tag{5}$$

is a critical electric field corresponding to the transition between two distinct tunneling regimes, which we consider below.

The first is the *Boltzmann limit*, $F\ll F_c$. Because the electric field is weak in this limit, the optimal energy must be close to E_1. For these energies, the exponent in the denominator on the right-hand side of Eq. (4) is negligibly small. Physically, this means that tunneling occurs from the Boltzmann tail of the Fermi distribution (regime of thermionic emission[15]). In this limit, the asymptotical solution of Eq. (4) is easily shown to be

$$\varepsilon_0(F)=E_1-\frac{(e\hbar F)^2}{8mk^2T^2}=E_1\left(1-\frac{F^2}{F_c^2}\right). \tag{6}$$

Now we expand all of the exponents in Eq. (2) in the vicinity of ε_0. This reduces the integrand in Eq. (2) to a Gaussian function that can easily be integrated to give

$$j_B(F)=\frac{e^2}{h^2}F\sqrt{2\pi mkT}\exp\left[-\frac{E_1}{kT}+\frac{(e\hbar F)^2}{24m(kT)^3}\right]. \tag{7}$$

Next we consider the second tunneling regime. This is the *Fermi limit* $F\gg F_c$, which is similar to field emission.[16] In this regime

$$\varepsilon_0(F)=-kT\ln(F/F_c), \tag{8}$$

and tunneling occurs mainly from states that lie just below the emitter Fermi level. Eq. (8) enables us to evaluate the integral over ε in Eq. (2) analytically giving

$$j_F(F)=\frac{e^2}{h^2}\sqrt{\frac{\pi mk^2T^2}{E_1}}\sqrt{\frac{F}{F_c}}\exp\left(-\frac{2E_1}{3kT}\frac{F_c}{F}\right). \tag{9}$$

Eqs. (7) and (9) give the injection current flowing through the tunnel barrier in the limiting cases of weak and strong electric fields, respectively. Note that in the theory of the Schottky barrier, the limiting regimes (thermionic and field emission) correspond to different doping densities in the semiconductor contacts rather than different values of the applied voltage. This leads to current-voltage characteristics for the Schottky diode that are different to those of the SL considered in the present paper.

The transition between the Boltzmann and the Fermi tunneling regimes occurs over a range of electric fields close to F_c. This critical field is given by Eq. (5) and depends on the parameter E_1. From this dependence, we can estimate F_c from the experimental $I(V)$ curves. Since the tunneling current has different exponential asymptotes [Eqs. (7) and (9)] in the low- and high-voltage limits, in Fig. 4 we plot the logarithm of the conductance, $\ln(I/V)$, using the experimental data shown in Fig. 2 for $B=0$. The curvature of this plot (Fig. 4) changes from concave to convex as V is increased. The concave part of the curve at low voltages corresponds to the Boltzmann regime of tunneling, where $\ln(I/F)\propto F^2$ [see Eq. (7)] . At higher voltages the curve becomes convex as a consequence of the $\ln(I/F)\propto 1/F$ dependence that characterizes the Fermi regime [see Eq. (9)]. The transition between these two regimes occurs at the voltage $V_c\approx 13$ mV marked in Fig. 4, which corresponds to $F_c=0.5$ kV/cm. Evaluating E_1 from E_c using Eq. (5) gives $E_1\approx 3$ meV. This is much lower than the E_1 value of 12 meV that follows from the band-structure calculations for an infinite SL. We attribute this difference to the fact that the conventional concept of a continuum miniband applies to a SL with an infinite number

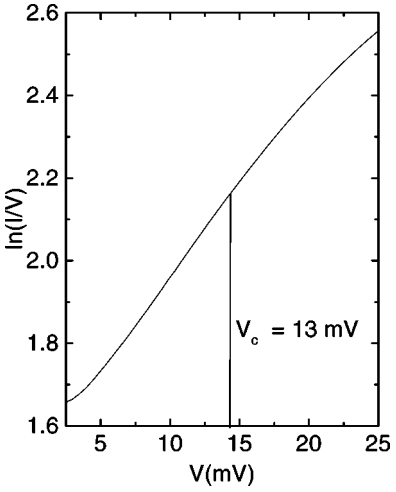

FIG. 4. Logarithm of conductance measured for the SL at $B=0$ T. The voltage V_c where the curvature changes sign (shown by the vertical line) marks the transition from the Boltzmann to the Fermi tunneling regimes.

of periods, whereas ours only has 19. The energy range of the miniband will be affected by the finite size of the SL and also by the effects of surface states and inhomogeneous diffusion of dopants from the contacts.

Our estimate of E_1 shows that the results of band-structure calculations for an infinite SL should be used with caution for finite samples, at least for an undoped SL. Finally, we note that the asymptotic formulas Eqs. (7) and (9) are only valid far from the transition voltage V_c. Therefore, only the low- and high-voltage parts of the curves shown in Fig. 4 follow these analytical formulas.

IV. SUPPRESSION OF THE TUNNELING CURRENT BY A MAGNETIC FIELD

A magnetic field applied parallel to the SL axis has no influence on the tunneling probability $D(\varepsilon)$ given by Eq. (1). However, we will now show that it does affect the distribution function $f(\varepsilon)$, and thereby suppresses the tunneling current obtained from Eq. (2). In a magnetic field, the electron states in the emitter contact associated with in-plane (y,z) motion are quantized into Landau levels with energies $\varepsilon_n=\hbar\omega_c(n+1/2)$, where $\omega_c=eB/m$ is the cyclotron frequency. If the electron scattering rate is ν, each Landau level has a finite width $\approx\hbar\nu$, which for the sake of simplicity, we consider to be B independent. Assuming a Lorentzian line shape for each broadened Landau level, we find that in a magnetic field, Eq. (3) is replaced by

$$f(\varepsilon)=\frac{2m\omega_c}{h}\sum_{n=0}^{\infty}\int_0^{\infty}\frac{1}{\pi}\frac{(\hbar\nu/2)d\varepsilon_\perp}{(\hbar\nu/2)^2+(\varepsilon_\perp-\varepsilon_n)^2}\times\frac{1}{1+\exp[(\varepsilon+\varepsilon_\perp)/kT]}. \tag{10}$$

Substituting this formula into Eq. (2) we obtain an expression for the tunnel current that involves two integrations, one over ε and the other over the in-plane energy $\varepsilon_\perp$. Integration over the longitudinal energy ε can be performed in the same way as for $B=0$, namely, by expanding the integrand in the vicinity of the optimal tunneling energy. We find that the optimal energy for a given Landau level decreases with increasing B and is given approximately by $\varepsilon_0^n(F,B)=\varepsilon_0(F)-(n+1/2)\hbar\omega_c$. Consequently, electrons in the lowest Landau level have the highest tunneling energy (energy of longitudinal motion), and therefore, dominate the current. In the limiting regimes of Boltzmann and Fermi tunneling, asymptotical calculations lead to formulas for the tunnel current density, which differ from Eqs. (7) and (9) only by a B-dependent factor, that is

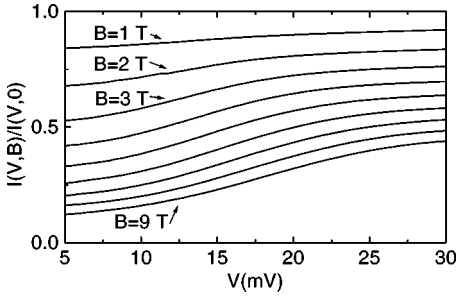

FIG. 5. Series of normalized current-voltage characteristics, $I(V,B)/I(V,0)$, measured for $B=1,2,\ldots,9$ T.

$$j(F,B)=j(F)q(B), \tag{11}$$

where

$$q(B)=\frac{\hbar\omega_c}{kT}\sum_{n=0}^{\infty}\int_0^{\infty}\frac{1}{\pi}\frac{(\hbar\nu/2)}{(\hbar\nu/2)^2+(\varepsilon_\perp-\varepsilon_n)^2}\times\exp\left(-\frac{\varepsilon_\perp}{kT}\right)d\varepsilon_\perp. \tag{12}$$

Note that in Eq. (11) we have omitted the subscripts that identify the Boltzmann and Fermi limits. The factor $q(B)$ describes the magnetosuppression of the tunnel current. Within the accuracy of our asymptotical calculations the current is suppressed uniformly, that is, the suppression ratio $j(F,B)/j(F,0)$ is independent of F. To compare this theoretical result with our experimental data, in Fig. 5 we plot normalized $I(V,B)/I(V,0)$ current-voltage characteristics obtained experimentally for different magnetic fields. The figure shows that indeed the variation of the normalized current with voltage is rather weak for magnetic fields $\leqslant 5$ T. In particular, the fractional variation of $I(V,B)/I(V,0)$ over the voltage range shown in Fig. 5 is always less than 0.2. At higher fields, the variation is stronger. This is because the peak in the $I(V)$ characteristics shifts to lower voltages with increasing B (see the inset in Fig. 2). Here we do not discuss the physical origin of this shift, but we do emphasize its effect on the form of $I(V,B)/I(V,0)$. In the vicinity of the peak the asymptotic formulas that lead to Eq. (11) are invalid. Because the peak shifts to lower V as B increases, the

range of voltages in Fig. 5 where the suppression is homogeneous, that is $I(V,B)/I(V,0)$ is constant, becomes narrower with increasing B.

The factor $q(B)$ given in Eq. (12) can be simplified if we assume that the broadening of the Landau levels is much larger than the energy of the thermal fluctuations, that is $\hbar\nu \gg kT$. We estimate that the scattering rate ν due to ionized impurities in the heavily doped emitter contact is approximately 6×10^{12} s^{-1} at $T=4.2$ K. Then $\hbar\nu/kT\simeq 14$. Because of the exponential factor in the integrand of Eq. (12), the principal contribution to the integral over $\varepsilon_\perp$ comes from a narrow range of energies close to $\varepsilon_\perp \sim kT$. If B is sufficiently large that $\hbar\omega_c > kT$, the Lorentzian factor can be considered as a constant since it varies slowly on a scale of kT. Then, after simple algebra, we obtain,

$$q(B) \cong \frac{\hbar\omega_c}{kT}\sum_{n=0}^{\infty}\frac{(\hbar\nu/2)}{(\hbar\nu/2)^2+\varepsilon_n^2}\int_0^\infty \exp\left(-\frac{\varepsilon_\perp}{kT}\right)d\varepsilon_\perp = \frac{1}{2}\tanh\left(\frac{\pi\nu}{2\omega_c}\right). \tag{13}$$

Note that this formula gives $q(0)=1/2$ rather than the correct value of 1 because it is invalid in the limit $B\to 0$.

For completeness we now give the expression for $q(B)$ in the limit $\hbar\nu \ll kT$, but note that this regime is not attained in the experiments. In this case, the Lorentzian factors can be replaced by delta functions, yielding the result

$$q(B) = \frac{\hbar\omega_c}{kT}\sum_{n=0}^{\infty}\exp\left(-\frac{\varepsilon_n}{kT}\right) = \frac{\hbar\omega_c/2kT}{\sinh(\hbar\omega_c/2kT)}. \tag{14}$$

Since the function on the right-hand side of Eq. (14) decays exponentially with increasing magnetic field, the current suppression in this case is much stronger than that given by Eq. (13). For example, when $B=3$ T, Eq. (14) gives $q(B)\approx 0.01$. Such strong suppression has never been observed in our experiments. By contrast, the weaker magnetosuppression given by Eq. (13) describes the experimental results rather well. This demonstrates that Landau-level broadening has a major effect on the observed magnetosuppression of the current.

The origin of this suppression has a clear physical explanation. When $B=0$, the principal contribution to the tunneling current is made by electrons with the optimal tunneling energy $\varepsilon_0(F)$ associated with motion along the SL axis, and with $p_y^2+p_z^2=0$. The external magnetic field **B** does not change the total electron energy, but it reduces the energy of the longitudinal motion at least by $\hbar\omega_c/2$. This is because, for nonzero B, the minimum energy for motion in the $y-z$ plane is increased to $\hbar\omega_c/2$. To maintain the state occupancy, the optimal tunneling energy must therefore fall by approximately the same value. This reduces the barrier transmission coefficient and so suppresses the current.

V. EFFECTS OF THE SPACE CHARGE ON THE CURRENT-VOLTAGE CHARACTERISTICS OF A FINITE-LENGTH SL

So far, we have considered how electrons are injected into the lowest SL miniband. But to calculate $I(V)$, we must also determine the electric-field profile along the SL. This profile depends in part on the conductivity of the SL itself that determines the space-charge distribution of electrons in the SL miniband. In an infinite model SL, the electric field is assumed to be homogeneous. However, this model is unrealistic since it does not include the emitter and collector contacts. Since we consider a real sample with contacts, space-charge effects are important, and can produce an inhomogeneous electric field.[22] The current-voltage characteristics Eqs. (7), (9), and (11) give the tunnel current as functions of the electric-field F in the tunneling region ($x<x_0$), *not* as functions of the applied voltage V. If the effects of the space charge are weak, then $V=FL$, where L is the distance between the n^+ contacts. However, in general, such a simple relation between F and V is not valid, and the electric-field profile $F(x,V)$, which depends parametrically on V, must be calculated self consistently. Once $F(x,V)$ is known, the $I(V)$ characteristics of the device can be obtained by substituting the electric-field $F_0 \equiv F(0,V)$ at the point of injection into the $j(F)$ characteristics of the tunneling contact given by Eqs. (7), (9), and (11).

In order to calculate $F(x,V)$, we have developed a realistic physical model of the SL's used in our experiments. The main features of this model are as follows: (i) The tunnel contact [consisting of the emitter contact and the SL region for $x<x_0$ (Fig. 3)], and that part of the SL layers with $x>x_0$, will be considered as two resistors connected in series. The current through any cross-section of the SL is equal to the current flowing through the tunnel contact. (ii) The effective length of the tunnel contact equals the length of the tunneling trajectory, $x_0=x_0(F)$ (see Fig. 3). This length is $x_0=(e\hbar^2/8mk^2T^2)F_0(V)$ for the Boltzmann tunneling regime, and $x_0=E_1/eF_0(V)$ for the Fermi regime. The length of the active part of the SL (where electrons have sufficient energy to enter the first miniband) is $L-x_0$. (iii) Current flow through the SL originates only from those electrons that are injected through the tunnel contact, i.e., there are no intrinsic carriers in the SL, which is nominally undoped. Due to the tunneling injection process, all electrons enter the SL at the bottom of the lowest miniband.

To obtain quantitative results from this model we need to determine the x dependence of the local volume density $N(x)$ of conduction electrons in the SL, which is related to $F(x,V)$ by Poisson's equation. These functions must be calculated self consistently from the current-conservation condition

$$j(F_0) = eN(x)v_d[F(x,V)], \tag{15}$$

where v_d is the local electron drift velocity, and the Poisson equation

$$\frac{dF(x,V)}{dx} = -\frac{eN(x)}{\epsilon\epsilon_0}. \tag{16}$$

Here, ϵ is the relative permittivity of GaAs. The right-hand side of Eq. (15) gives the current at a position x inside the active part of the SL. It is expressed in a Drude formalism, and is proportional to the drift velocity of conduction electrons v_d, which is a nonlinear function of $F(x,V)$. The simple Esaki-Tsu model[1] gives

$$v_d(F)=v_0\frac{F(x,V)/F^*}{1+[F(x,V)/F^*]^2}, \tag{17}$$

where $v_0=\hbar/(m_{sl}d)$ in which the effective mass m_{sl} is inversely proportional to the second derivative of the miniband energy wave-vector dispersion relation at the bottom of the miniband, and $F^*=3.8$ kV/cm is the electric field corresponding to the peak in the current-voltage characteristics at $B=0$.

Eqs. (15) and (16) are subject to two boundary conditions. One is the continuity of the electric field at the point $x=x_0(F)$ where the electrons enter the SL miniband. At this point

$$F_0=F(x_0,V). \tag{18}$$

The second boundary condition establishes the relation between the distribution of the electric field in the device and the applied voltage, which requires that

$$V=V_s+x_0F_0+\int_{x_0}^{L}F(x,V)dx, \tag{19}$$

where $V_s\propto V$ is the voltage dropped across the undoped spacer layers adjacent to the emitter and collector contacts. Since these spacer layers are short (10.2 nm), V_s can be neglected at voltages below ≈ 35 mV. At higher voltages, V_s becomes important, but then the electron injection process is completely different from the tunneling mechanism considered here. The reason for this is that the electrons gain energy from the electric field when they pass through the emitter spacer layer. For $V\geqslant 35$ mV this energy is sufficient to overcome the triangular barrier of height ~ 3 meV shown in Fig. 3. Then the electrons enter the lowest miniband directly from the emitter contact, and the $I(V)$ characteristic is controlled by miniband transport alone. The magnetosuppression of $I(V)$ observed in this high-voltage range can be explained by considering the influence of B on the electron-scattering rate in the miniband.[12–14]

Eqs. (15)–(19) form a closed self-consistent set of equations. To obtain the current-voltage characteristics, we must first determine $F_0(V)$ from these equations. This is done in three steps. First, the concentration $N(x)$ obtained from Eq. (15) is substituted into Eq. (16). This gives a first-order nonlinear differential equation for $F(x,V)$. The second step is to solve this equation subject to the boundary condition Eq. (18), and then substitute the solution into Eq. (19). This provides an implicit equation for $F_0(V)$. The third step is to solve this equation numerically in order to determine $F_0(V)$. In Figs. 6 and 7 we show the relation between F_0 and V for the Boltzmann and Fermi tunneling regimes, respectively. Along the horizontal axis in each figure we plot the product

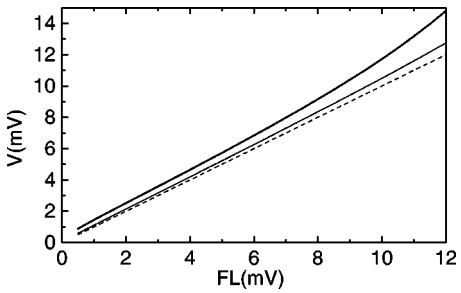

FIG. 6. Calculated applied voltage V plotted as a function of the effective voltage $F_0(V)L$ for the Boltzmann tunneling regime. The thick solid curve is for $B=0$ T and the thin solid curve is for $B=10$ T. These curves are nonlinear due to the inhomogeneity of the electric field in the SL. Curves for intermediate magnetic fields, $B=1,2,\ldots,9$ T, lie in between the thin and the thick solid lines. The dashed line shows the linear variation of $F_0(V)L$ with V obtained when space-charge effects are neglected.

$F_0(V)L$, which shows the effective voltage that would be dropped across the device if the electric field were independent of x.

These graphs show that $F_0(V)$ becomes increasingly nonlinear as V is increased and the effects of space-charge buildup become more important. The effective voltage F_0L is always lower than V because the electric field in the tunnel contact F_0 is lower than the mean electric field V/L. The physical reason for this difference is the negative space charge accumulated in the SL. Because of this space charge, the electric field in the SL layers increases with increasing x. The local electric field F_0 must therefore be smaller than the mean field V/L in order to ensure that the total voltage dropped across the device equals the applied voltage V. As a consequence, our calculated $I(V)$ curves increase more slowly with increasing V when the effects of space charge buildup are taken into account. This can be seen from Fig. 8 in which we plot $I(V)$ characteristics calculated for a mesa with a cross-sectional area of 7.8×10^{-3} mm^2 including (curves with square symbols) and neglecting (curves with circles) space charge effects. We consider two magnetic-field values, $B=0$ T [Figs. 8 (a) and (c)] and $B=10$ T [Figs. 8(b) and (d)]. We also consider both the low-voltage Boltzmann tunneling regime [Figs. 8(a) and (b)] and the high-voltage Fermi regime [Figs. 8(c) and (d)]. For both voltage ranges and both magnetic-field values, the calculated current increases more slowly with increasing V when space-charge

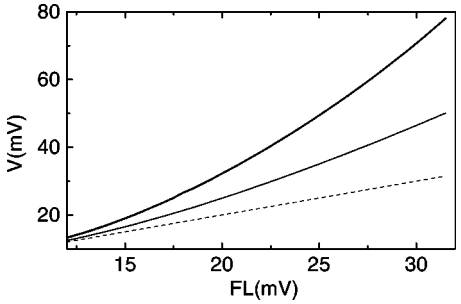

FIG. 7. The same as Fig. 6 but for the Fermi tunneling regime.

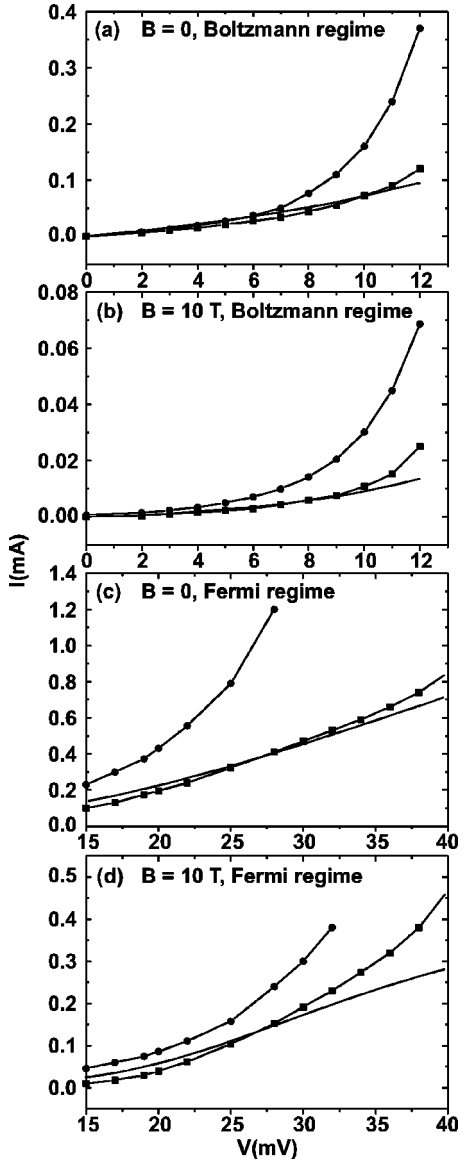

FIG. 8. $I(V)$ characteristics in the Boltzmann [(a) and (b)] and Fermi [(c) and (d)] tunneling regimes with $B=0$ [(a) and (c)] and $B=10$ T [(b) and (d)]. Solid curves without symbols show experimental data. Squares (circles) indicate $I(V)$ curves calculated including (neglecting) the effects of space-charge buildup in the SL miniband.

buildup is included in the calculations. Note that the effect of this space charge becomes more pronounced as V increases. This is because the tunnel current from the emitter into the MB increases exponentially with increasing V, while the Drude current within the SL layers increases more slowly. Consequently, to ensure current conservation, the occupancies of the MB states and corresponding space charge must increase with increasing V. This effect is clearly seen by comparing the effective voltages shown in Figs. 6, 7. In the Boltzmann regime (Fig. 6) where space-charge effects are less important, the effective voltage F_0L deviates much less from V, than in the Fermi regime (Fig. 7).

When space-charge effects are included, we obtain good agreement between the theoretical $I(V)$ plots (solid curves with square symbols in Fig. 8) and the corresponding experimental data (solid curves with no symbols in Fig. 8) for both $B=0$ T [Figs. 8(a) and (c)] and $B=10$ T [Figs. 8(b) and (d)]. Similar correspondence is obtained for all $B<10$ T, which strongly supports the proposed mechanism of magnetosuppression.

It is easy to see that Eqs. (7) and (9) do not give the same current at $F=F_c$. As a consequence of this mismatch, the theoretical $I(V)$ curves rise above the experimental data near $V=V_c=13$ mV in Boltzmann regime [Figs. 8(a) and (b)], but fall below them in Fermi regime [Figs. 8(c) and (d)]. Although the asymptotic formulas Eqs. (7) and (9) give poor approximations to the current in the vicinity of the transition voltage V_c, the good agreement between the theoretical and experimental $I(V)$ curves found away from V_c suggests that our estimate of V_c itself is fairly accurate. Since the calculated current is very sensitive to the value of V_c, any significant error in our estimate of this parameter would produce much worse agreement between theory and experiment.

In Figs. 8(c) and (d), the calculated $I(V)$ curves deviate strongly from the experimental data for $V>35$ mV, even when space-charge effects are included. This is because, as mentioned above, the transmission coefficient of the triangular potential barrier shown in Fig. 3 becomes close to unity at high V, and so the electrons are able to enter the miniband directly. In this region, the conductivity of the SL is explained well by a velocity quenching model[13] and related Monte Carlo simulations.[14]

VI. CONCLUSION

In summary, we have shown that the magnetosuppression of SL miniband conduction observed in our experiments can be explained by considering tunneling injection processes that transmit electrons from the doped emitter contact into the SL layers. To enter the SL miniband, the electrons need to tunnel through the potential barrier that is formed if the lowest miniband lies above the emitter Fermi level. At helium temperatures, the height of this barrier greatly exceeds kT and the optimal tunneling energy is obtained by maximizing the product of the electron distribution function and the tunneling transmission coefficient. When a magnetic field is applied along the SL axis, the in-plane motion is quantized into Landau levels. As a consequence, the optimal tunneling energy and corresponding transmission coefficient both fall and thereby suppress the current. Our calculations of the $I(V)$ characteristics, based on this mechanism of injection, are in good agreement with the corresponding experimental data for a wide range of V and B values.

ACKNOWLEDGMENTS

This work was supported by EPSRC, The Royal Society, and by CONACyT (Mexico).

*On sabbatical leave from Instituto de Física, UAP, Apdo. Post. J-48, Puebla 72570, Mexico
[1] L. Esaki and R. Tsu, IBM J. Res. Dev. **14**, 61 (1970).
[2] L. Canali, M. Lazzarino, L. Sobra, and F. Beltram, Phys. Rev. Lett. **76**, 3618 (1996).
[3] J. Lui, E. Gornik, S. Xu, and H. Zheng, Semicond. Sci. Technol. **12**, 1422 (1997).
[4] N. H. Shon and H. N. Nazareno, Phys. Rev. B **55**, 6712 (1997).
[5] P. Kleinert and V. V. Bryksin, Phys. Rev. B **56**, 15 827 (1997).
[6] V. V. Bryksin and P. Kleinert, Physica B **269**, 163 (1999).
[7] V. J. Hales, R. J. Nicholas, and N. J. Mason, in *Proceedings of the 25th International Conference on Physics and Semiconductors* (Osaka, Japan, 2000), part II, p. 485.
[8] H. Noguchi, H. Sakaki, T. Takamasu, and N. Miura, Phys. Rev. B **45**, 12 148 (1992).
[9] W. M. Shu and X. L. Lei, Phys. Rev. B **50**, 17 378 (1994).
[10] A. Sibille, J. F. Palmier, A. Celeste, J. C. Portal, and F. Mollot, Europhys. Lett. **13**, 279 (1990).
[11] H. J. Hutchinson, A. W. Higgs, D. C. Herbert, and G. W. Smith, J. Appl. Phys. **75**, 320 (1994).
[12] H. M. Murphy, L. Eaves, A. Nogaret, S. T. Stoddart, P. C. Main, M. Henini, N. Mori, C. Hamaguchi, D. K. Maude, and J. -C. Portal, Microelectron. Eng. **47**, 65 (1999).
[13] L. Eaves *et al.*, Physica B **272**, 190 (1999).
[14] N. Mori, C. Hamaguchi, L. Eaves, and P. C. Main (unpublished).
[15] C. B. Duke, in *Solid State Physics*, Suppl. 10, edited by F. Seitz, D. Turnbull, and H. Enrenreich (Academic Press, New York, 1969).
[16] F. A. Padovani, in *Semiconductors and Semimetals*, edited by R. K. Willardson and A. C. Beer (Academic Press, New York, 1971), Vol. 7, Pt. A.
[17] J. M. Ziman, *Principles of the Theory of Solids* (Cambridge University Press, Cambridge, England, 1972).
[18] A. Sibille, J. F. Palmier, and F. F. Laruelle, Phys. Rev. Lett. **80**, 4506 (1998).
[19] A. Vagov and F. Kusmartsev (unpublished).
[20] S. G. Christov, Phys. Status Solidi **17**, 11 (1967).
[21] R. Stratton, Phys. Rev. **125**, 67 (1962); F. A. Padovani and R. Stratton, Solid-State Electron. **9**, 695 (1966).
[22] M. Cahay, M. McLennan, S. Datta, and M. S. Lundstrom, Appl. Phys. Lett. **50**, 612 (1987).